JOURNAL OF APPLIED ELECTROCHEMISTRY **27** (1997) 1369–1379

On unsteady electrochemical coating of a cylinder at moderately large Reynolds number

P. OLIVAS*

Royal Institute of Technology, Department of Mechanics, S-100 44 Stockolm, Sweden

S. ZAHRAI

ABB Corporate Research, S-721 78 Västerås, Sweden

F. H. BARK

Royal Institute of Technology, Department of Mechanics, S-100 44 Stockolm, Sweden

Received 20 August 1996; revised 29 May 1997

Electrodeposition on a circular cylinder under forced convection was simulated for Reynolds numbers 10 and 200 by numerical solutions of the incompressible Navier–Stokes and mass transport equations. Current density distribution and concentration fields were computed with changing mass transfer and flux rates. Comparisons with earlier numerical and theoretical results are presented for Reynolds number 10. It is shown that the unsteady wake that appears for Reynolds numbers greater than 50 affects the mass transfer from the surface of the cylinder only in an average sense. This result is compared with a heat transfer case, where unsteadiness is much more manifest.

Keywords: *electrodeposition*, *electrochemical coating*, *forced convection*, *cylinder*, *mass transport*, *numerical solutions*

1. Introduction

The technique of electrolytic deposition of thin metal coatings to other metals evolved during the middle of the last century. This technology has been successfully used for development of new products with unique functional properties. Today it is one of the highest volume chemical technologies; and most metalworking plants have in-house plating shops. More recently, the demands on quality and properties of metal coatings have increased significantly.

Electroplating processes are mainly used in the surface finishing industries for items such as printed circuit boards, magnetic alloys for computer memories, coatings for hard disk drives, wear resistant coatings, corrosion resistant alloys, electroreformed laser mirrors, contacts/connectors and decorative coatings [1,2]. Many factors can affect the rate of an electrodeposition reaction. The imposed electric potential, electrode parameters (material composition, surface state, geometry etc.) and electrolyte parameters (composition, concentrations, conductivity, velocity, temperature etc.) are examples of such factors [3]. Parametric adjustment of an electroplating line is, therefore, a formidable task, which so far has been dealt with on empirical basis [4]. But with the increasing requirements on quantity, quality and productivity, the purely empirical approach to the optimization problem needs to be supplemented with theoretical estimations and computations based on first principles.

Forced convection is commonly used in electroplating processes. For example, the electrolyte may be pumped through a cell. Other examples are stirring by air bubbles or by mechanical agitation. In many electroplating processes a continuous strip or wire or an array of workpieces moves through an electroplating bath. The motion of the material to be plated generates a flow pattern that enhances mass transfer which, in turn, leads to more efficient plating. In such cases, high reaction rates are imposed [5]. The hydrodynamics is then of particular importance as the current distribution is determined by the forced convective mass transport of reactant. Convection–diffusion theory in its classical form is well known and available for the reader in standard textbooks [6,7]. However, at the present time, there are no practical tools that are useful for prediction of electroplating.

Levich [6] remarked that the convective–diffusion transport of ions in electrolytes is characterized by large Schmidt numbers ($\sim 10^3$) and is thus akin to heat transport at large Prandtl numbers. Lighthill [8] developed an approximative analytic solution for steady heat transfer from bodies at high Prandtl numbers in the case of forced convection. Acrivos [9]

* Also at Laboratoire des Ecoulements Géophysiques et Industriels, Institut de Mécanique de Grenoble, B.P. 53 X, 38041 Grenoble Cedex, France.

0021-891X

applied the method devised by Lighthill to a wide range of problems. The key element of Lighthill's method is that the concentration distribution, and thus the rate of mass transfer, can be computed approximately in analytic form if the velocity field near the electrode is known. The one-to-one correspondence between mass transfer and velocity gradient is the basis for electrochemical methods for wall shear stress measurements [10, 11].

In the present work electrochemical mass transfer to a circular cylinder oriented perpendicular to a moving electrolyte is studied. At large distances from the cylinder, the velocity of the electrolyte is constant. This case is of canonical type because of the simplicity of the boundary conditions, the complexity of the physico-chemical processes, the fundamental mechanisms exhibited and numerous industrial applications. One example of practical applications is the production of gold plated electrical connectors.

The nature of the flow pattern around a cylinder depends on the Reynolds number Re, for example [12, 13]. In most investigations of the unsteady regime attention is focused on the unsteady behaviour of the vortices downstream the cylinder rather than the properties of the flow close to the surface of the cylinder.

For theoretical predictions, since the governing equations are nonlinear and exact solutions are not available, numerical methods have been used in a number of investigations to deal with heat transfer from a circular cylinder. Žukauskas [14] has given an extensive review of published data and proposed several empirical correlations between heat transfer rates and flow variables.

For electrochemical mass transfer to a circular cylinder, comparatively few investigations are reported. Most of these focus on the overall mass transfer [15, 16]. In several studies, the microelectrode technique, which relies on the fact that unsteady mass diffusion at high Schmidt number close to a solid surface depends only on the locally linear tangential velocity component, has been made use of to measure the local shear stress on the cylinder [11, 17, 18].

For rough estimates, the classical Nernst diffusion layer model is often adopted for the complex velocity and concentration profiles near the cathode surface, see [19, 20, 21]. In this model, it is assumed that the motion of the electrolyte near the surface of the electrode can be divided into two zones. Close to the surface it is assumed that there is a thin layer which is totally stagnant such that diffusion is the only mode of mass transport. At steady state, the concentration profile is then linear. Outside this layer, only convection is assumed to be of importance and the concentration is, on an ad hoc basis, taken to be equal to that of far field. In a real flow, however, a sharp limit cannot be observed due to diffusion of momentum [21]. Nevertheless, the Nernst model has been found useful for coarse approximations.

Numerical analysis has so far not been in widespread use for investigation of convection–diffusion problems at high Schmidt numbers. Josserand [18] studied the mass transfer to a circular cylinder at $Re = 10$ and $Re = 5 \times 10^4$. He used a simplified model for the velocity field close to the cylinder. At $Re = 10$ the wall vorticity distribution was taken from the numerical study by Dennis *et al.* [22], and at $Re = 5 \times 10^4$ from the experimental data reported by Son and Hanratty [23]. In both cases a linear velocity profile was then imposed close to the surface of the cylinder. The concentration field was then computed numerically. Although limited, the investigation of Josserand was pioneering regarding the use of numerical methods for simulation of electroplating processes. The aim of this work is to make a detailed numerical investigation of electroplating of male electrical contacts.

2. Problem statement

The specific case to be studied in this work, gold plating of male electric contacts, is chosen due to its industrial importance. Usually, in the industrial process, an array of cylinders is moving through a series of baths [11, 24]. In this study, however, as a first step, the plating process of a single cylinder is considered.

Gold plating solutions usually include a supporting electrolyte. The ions of the supporting electrolyte have a larger mobility than the reactant and are responsible for the transport of charge outside the mass transfer boundary layer. Consequently, the electric field is reduced in the electrolyte and the fraction of the net charge transport carried by the reacting ions is negligible. The electrical potential can be considered as constant in the bath. The concentration will be the only factor producing nonuniformity in the current distribution around the surface of the cylinder [6, 19, 21].

The mathematical problem for plating of a cylinder is reduced to the computation of forced convective transport of reactant to the surface of the cylinder. The system of equations to be solved for the velocity field $\boldsymbol{u}$ and the pressure field p, are the Navier–Stokes equations

$$\frac{\partial \boldsymbol{u}}{\partial t} + \boldsymbol{u} \cdot \nabla \boldsymbol{u} = -\frac{1}{\rho}\nabla p + \nu \nabla^2 \boldsymbol{u} \tag{1}$$

and the continuity equation for incompressible flow

$$\nabla \cdot \mathbf{u} = 0 \tag{2}$$

As forced convection is considered, when $\boldsymbol{u}$ has been computed from Equations 1 and 2, the concentration c of the solute can be computed from the conservation equation

$$\frac{\partial c}{\partial t} + \boldsymbol{u} \cdot \nabla c = D \nabla^2 c \tag{3}$$

The boundary conditions on the cathodic cylinder wall are

$$\boldsymbol{u} = \vec{0} \quad \text{and} \quad D\,\hat{n} \cdot \nabla c = k\,c \tag{4}$$

In these expressions $\hat{n}$ is the unit vector normal to the cylinder and the rate of reaction k taken as a constant on the cylinder wall. In Equations 1 and 3, ν is the

kinematic viscosity of the electrolyte, ρ its density and D the solute diffusion coefficient. Low values of k, on the one hand, imply that the charge transfer kinetics at the cathode controls the current density. High values of k, on the other hand, mean that the mass transfer is mainly controlled by the hydrodynamics, the transfer of reacting particles from the bulk to the near-wall region being the only limitation on particle deposition [6]. This parameter range, in which the concentration at the cathode surface is close to zero, is said to be mass transport limited. The current density on the cathode is slightly below the limiting-current density.

Far from the cylinder, the velocity field is taken to be uniform, that is,

$$\lim_{|\boldsymbol{X}|\to\infty} \boldsymbol{u} = U_0 \boldsymbol{u}_x \tag{5}$$

The normal velocity at the outlet was set so that the global conservation of mass was satisfied between the inlet and outlet, and a zero streamwise gradient was imposed for the remaining variables.

In the present work, the cylinder is assumed to be very long compared with its diameter thus permitting a two-dimensional treatment.

The diffusion coefficient of the diffusing solute, D, is assumed to be constant and has a low value ($D \sim 10^{-9}$–$10^{-10}\,\mathrm{m^2\,s^{-1}}$) compared to the fluid kinematic viscosity ($\nu \sim 10^{-6}\,\mathrm{m^2\,s^{-1}}$). This leads to high value of Schmidt number, Sc, that is,

$$Sc = \frac{\nu}{D} \geq 10^3 \tag{6}$$

The diffusion boundary layer is thus always nested within the hydrodynamic boundary layer. For typical electrolytes, the ratio between the thickness of the diffusion boundary layer and the hydrodynamic layer, respectively, is of the order of 10^{-1}[6].

The above set of equations can be transformed into a suitable nondimensional form by choosing the diameter of the cylinder, L, as the length-scale, the far field velocity, U_0, as the velocity scale, the concentration in the solution, C_0, as the concentration scale, L/U_0 as the time scale and ρU_0^2, the dynamic pressure, as the relevant scale for the pressure field. A mass transfer length scale is given by the quantity $\delta = (DL^2/U_0)^{1/3}$, which is obtained by balancing the convective mass flux in the tangential direction and diffusive mass flux in normal direction [18]. A scale for the reaction rate is then given by $k_0 = D/\delta$. The nondimensional versions of Equations 1–3 are

$$\frac{\partial u}{\partial x} + \frac{\partial v}{\partial y} = 0 \tag{7}$$

$$\frac{\partial u}{\partial t} + u\frac{\partial u}{\partial x} + v\frac{\partial u}{\partial y} = -\frac{\partial p}{\partial x} + \frac{1}{Re}\left(\frac{\partial^2 u}{\partial x^2} + \frac{\partial^2 u}{\partial y^2}\right) \tag{8}$$

$$\frac{\partial v}{\partial t} + u\frac{\partial v}{\partial x} + v\frac{\partial v}{\partial y} = -\frac{\partial p}{\partial y} + \frac{1}{Re}\left(\frac{\partial^2 v}{\partial x^2} + \frac{\partial^2 v}{\partial y^2}\right) \tag{9}$$

$$\frac{\partial c}{\partial t} + u\frac{\partial c}{\partial x} + v\frac{\partial c}{\partial y} = \frac{1}{Pe}\left(\frac{\partial^2 c}{\partial x^2} + \frac{\partial^2 c}{\partial y^2}\right) \tag{10}$$

The nondimensional boundary conditions on the cylinder are

$$u = 0, \quad v = 0 \tag{11}$$

$$P e^{-1/3}\,\frac{\partial c}{\partial r} = \kappa\, c \tag{12}$$

The Reynolds and Peclet numbers are defined as

$$Re = \frac{\rho U_0 L}{\mu} \quad \text{and} \quad Pe = \frac{U_0 L}{D} \tag{13}$$

No separate notation has been introduced for the nondimensional variables, except for the nondimensional reaction rate constant, that is, $\kappa = k/k_0$.

For the mass transport limitation case (i.e. large values of κ) the concentration boundary conditions at the cylinder wall is suitably written as

$$c = 0 \tag{14}$$

The finite computational domain is illustrated in Fig. 1. The origin of the cartesian coordinate system is at the centre of the cylinder. In terms of nondimensional units, the domain is defined as

$$-2.5 \leq x \leq 12.5 \quad \text{and} \quad -5 \leq y \leq 5 \tag{15}$$

where the x direction is parallel to the flow at far field. The following boundary conditions are prescribed at the inlet and outlet, that is, $x = -2.5$ and $x = 12.5$, respectively

$$u = 1, \quad v = 0, \quad c = 1 \tag{16}$$

$$\frac{\partial u}{\partial x} = 0, \quad \frac{\partial v}{\partial x} = 0, \quad \frac{\partial c}{\partial x} = 0, \quad p = 0 \tag{17}$$

On the boundaries of the computational domain parallel with the mean flow, the following boundary conditions are prescribed:

$$u = 1, \quad v = 0, \quad \frac{\partial c}{\partial y} = 0 \tag{18}$$

The problem was solved numerically for Reynolds numbers of 10 and 200 and a large value of the Schmidt number. The error made by restricting the simulations to two dimensions was deemed small as significant three-dimensional effects occur only when the Reynolds number exceeds 200 [13].

3. Methodology

The set of equations were solved numerically by using the commercially available numerical code, CFX F3D [25]. The solution methodology is based on the finite-volume discretization of the transport equations and the continuity equation for an incompressible fluid, resulting in a discrete set of equations for the velocity, pressure and concentration. F3D uses multi block structured grid system for modelling of complex geometries. All variables are defined at the centre of control volumes. To examine effects of the spatial resolution on the results, simulations were carried out using different computational meshes with number of elements varying from 7250 to 18 880. Finally, a grid with 9050 elements was chosen as finer meshes did not produce any noticeable change in the solution.

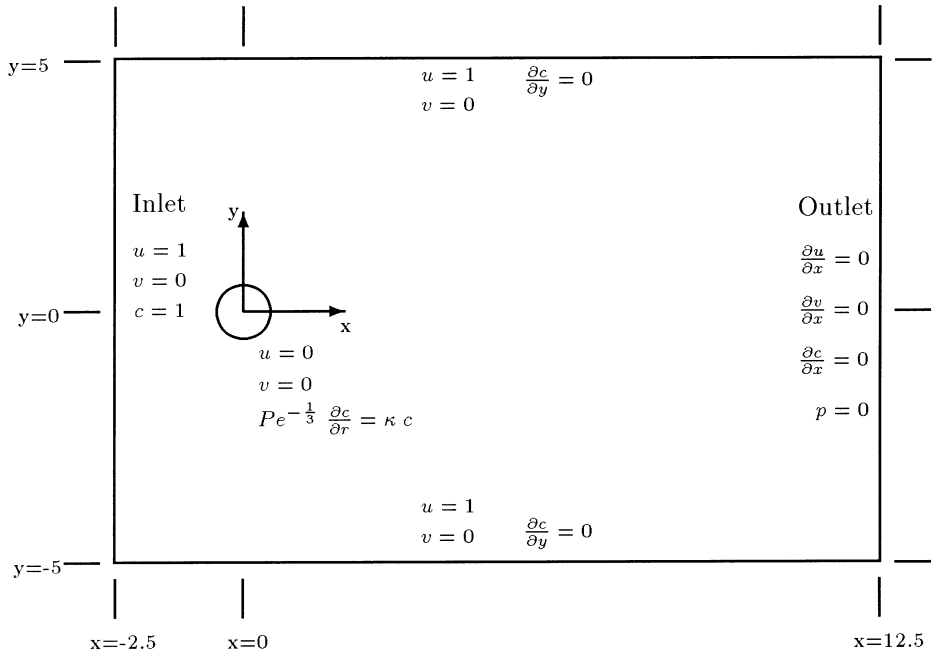

Fig. 1. Computational domain.

The numerical scheme is based on the pressure correction method where a correction to the pressure field is computed such that the divergence of the velocity field is forced to be zero and the continuity equation (2), can be satisfied. To avoid the spurious modes in the pressure field appearing when computing the velocity components on control volume faces from those on control volume centres, the Rhie and Chow interpolation scheme is used.

At each time step the nonlinear equations are solved by iteration. The convection velocity and other parameters are evaluated at the previous iteration and a linear equation system is formed for each variable. The linearized difference equation system is solved by an iterative solution method*.

The convective part of the equations was discretized by an upwind discretization. The use of a low order upwind method gives rise to a high numerical diffusion which suppresses the unsteadiness of the flow at a sufficiently high Reynolds number. To avoid this effect a third order quadratic upwind differencing (QUICK) scheme was used. However, in order to compare the results averaged in time with the steady solution of the governing equations the hybrid discretization, that is, a combination of the first order upwind differencing and the central differencing, was used to force the system to converge.

4. Results

The parameters in the present simulations were chosen to be as close as possible to available experimental data in the work of Josserand [18] and Olivas [11]. A cylinder of diameter 2 cm was assumed to be located in a bath of 10 diameters width. The electrolyte was an aqueous solution of potassium ferricyanide with sodium hydroxide as supporting electrolyte. At 30 °C, the physical properties of this solution are: density $\rho = 998.2\,\mathrm{kg\ m^{-3}}$, kinematic viscosity $v = 1.004 \times 10^{-6}\,\mathrm{m^2\,s^{-1}}$ and diffusion coefficient of ferricyanide ions in the electrolyte $D = 5 \times 10^{-10}\,\mathrm{m^2\,s^{-1}}$. The Schmidt number is 2010.

Although the main aim of this work was to investigate unsteady forced convection in the oscillatory separated flow around a circular cylinder (the Kármán vortex street) which is a distinct feature at moderately large Reynolds numbers of about 200, cases at lower values of Reynolds number have also been simulated in order to validate the computations by comparisons with earlier simulations.

In this Section, results for the steady flow at Reynolds number 10 are compared with previous work by Josserand [18]. Also results for the unsteady flow at Reynolds number 200 are presented, both for the mass transport controlled case and a case that is intermediate between control due to charge and mass transfer. Mass transfer results from a numerically enforced steady solution for the flow at Reynolds number 200 is compared with corresponding results from the time-averaged unsteady solution. At the end of this Section a comparison is made between the obtained results for mass transfer and a similar heat transfer case in water.

Mass transfer to a cylinder at $Re = 10$ has been computed approximately, using an *ad hoc* model, by Josserand [18], where nondimensional mass transfer rate, κ, was varied between 0.03, 0.3, 3 and 10^4. In the present work, the calculations were performed for five different values for κ, 0.03, 0.3, 3, 30, 300 and for the limiting-current state, that is, $c = 0$ at the surface of the cylinder.

* 'Full field Stone's method for the velocity variables and the concentration, 'preconditioned conjugate gradients' method for the pressure.

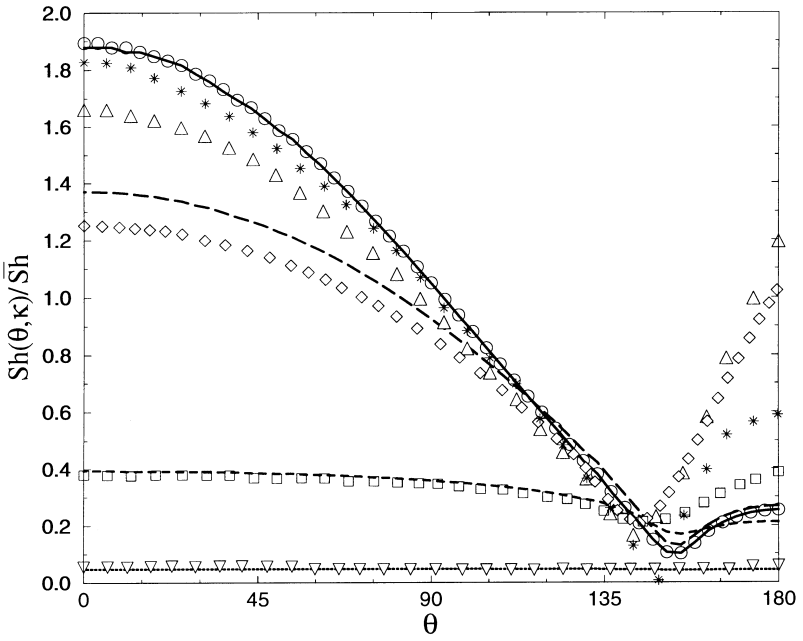

Fig. 2. Flux distribution around the cylinder, $Re = 10$. Present work: (○) limiting current, (—) $\kappa = 300$, (– – –) $\kappa = 3$, (- - -) $\kappa = 0.3$, (· · ·) $\kappa = 0.03$. Josserand [18]: (△) $\kappa = 1 \times 10^4$, (◇) $\kappa = 3$, (□) $\kappa = 0.3$, (▽) $\kappa = 0.03$. Lighthill's solution as calculated by Sobolík and Wein [26] : (∗) analytical at limiting current.

Figure 2 shows the nondimensional mass flux at the surface of the cylinder, in terms of the Sherwood number Sh ($Sh = \partial c/\partial r$ at the wall) normalized by the mean value of the Sherwood number over the cylinder ($\overline{Sh}$). The flux increases with the value of κ, tending towards the maximum value giving the limiting current. The minimum mass flux is, as expected, located at the separation point situated near 150°, where the supply of reactant is weakest, cf. Fig. 3.

For $\kappa = 300$, the local Sherwood number is, from a numerical point of view, practically equal to its maximum value (i.e. that for the limiting current). At the limiting current, the rate of electron transfer is fast compared with the reactant supply and the mass flux distribution is fully controlled by the convective–diffusive mass transport to the surface of the cylinder.

The results shown in Fig. 2 are in reasonable agreement with those obtained by Josserand [18]. In this graph, $\overline{Sh}$ is the angular average of Sh around the surface of the cylinder. It is worth noting that non-normalized flux distributions in the front part of the cylinder, (i.e. $\theta = 0° - 150°$) are in excellent agreement

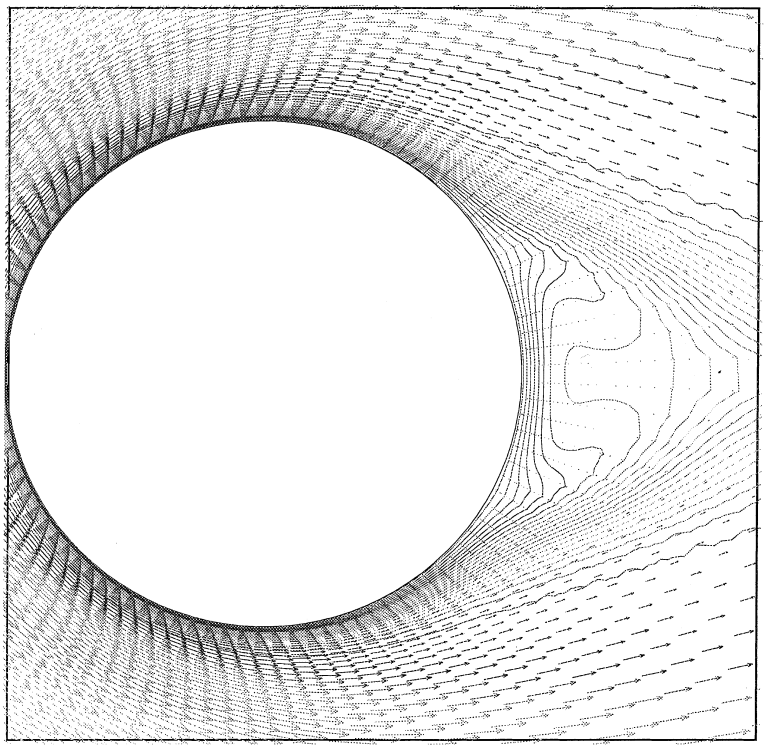

Fig. 3. Concentration and velocity fields. Limiting-current state at $Re = 10$.

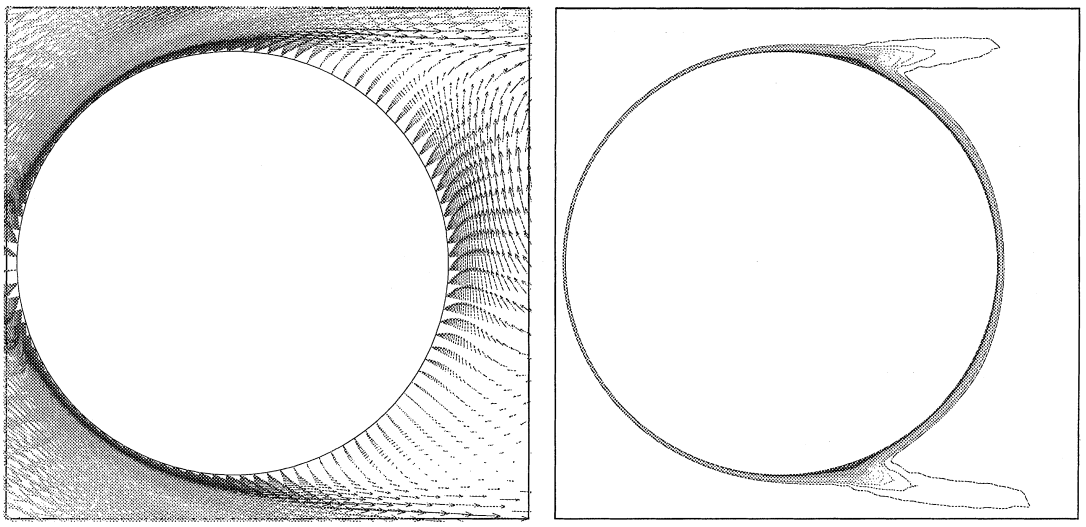

Fig. 4. Instantaneous velocity and concentration fields. Limiting-current state at $Re = 200$.

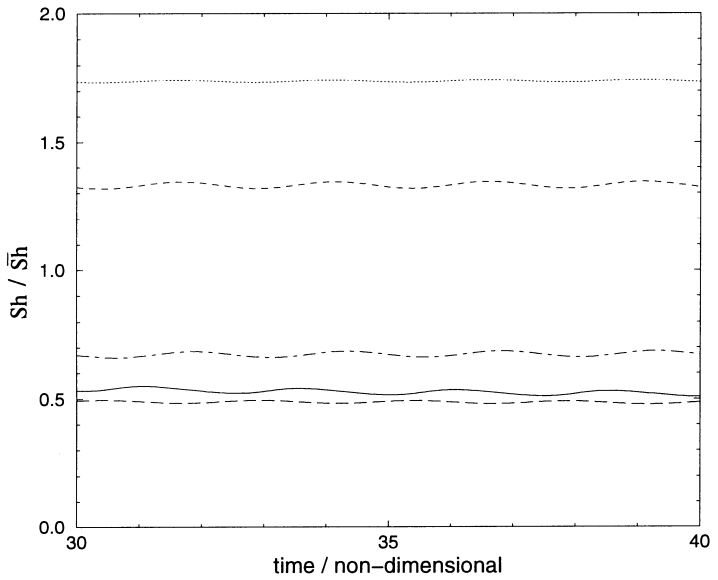

Fig. 5. Time-dependent flux distribution. Limiting-current state at $Re = 200$. Angular positions: (—) 151.2°, (– – –) 118.8°, (– - –) 90°, (- - -) 61.2°, (· · ·)28.8°.

with those computed by Josserand and the Lighthill's analytical solution. Deviations are found on the rear part of the cylinder. These deviations indicate that the linear approximation of the velocity field inside the diffusion layer is inaccurate for the rear part of the cylinder. This presumption appears to be supported by Fig. 3, which shows that the isoconcentration lines do not show boundary layer behaviour in this region. Convection is simply too weak outside the rear point of the cylinder for $Re = 10$. The mentioned deviations give slightly different values for $\overline{Sh}$.†

As the Reynolds number becomes sufficiently high, the wake becomes unsteady. An asymmetric eddy pattern appears, forming the well-known Kármán street [13] downstream of the cylinder. In the simulations, no artificial perturbation was introduced to generate the vortex shedding. A periodic flow was established spontaneously after a transition period. Computed Strouhal numbers for the vortex shedding are in good agreement with documented experimental results. Details of the hydrodynamics are given in the Appendix. Instantaneous isoconcentration lines for the $Re = 200$ unsteady case are shown in Fig. 4, with the corresponding velocity field. Note that this is an arbitrary phase of oscillation cycle; strong variation in the flow pattern can be observed. The time-dependent non-dimensional fluxes, the local Sherwood number, at different angular positions are presented in Fig. 5. The data in that figure are normalized by $\overline{Sh}$, the mean value of the Sherwood number over the cylinder averaged in time. It is interesting to note that the fluctuations of the local value of the Sherwood number is only about 1% of its time averaged value. In Fig. 6 the mass flux distribution and the magnitude of fluc-

† This results in differences in normalized profiles as can be seen in Fig. 2.

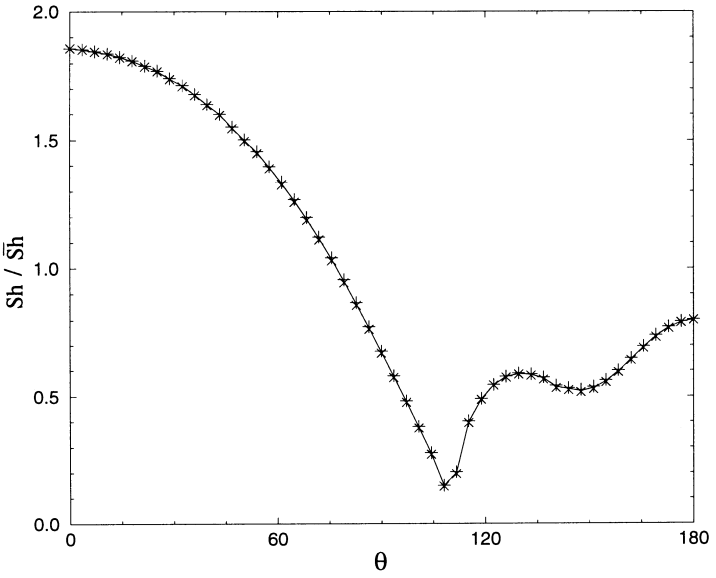

Fig. 6. Flux distribution around the cylinder. Limiting-current state at $Re = 200$. σ is the standard deviation. (–) mean, (+) mean $+\sigma/2$, ($\times$) mean $-\sigma/2$.

tuations are presented as three curves, the local time averaged and the local time averaged plus and minus half of the standard deviations. However, as can be seen in that Figure, the three curves are, for practical purposes, the same. The fact that the unsteady mass transfer hardly deviates at all from its mean value, even though the flow in the wake is certainly unsteady to lowest order, may be worth comment. An explanation for this somewhat surprising phenomenon can be found by considering time scales. It is well known that the period τ_s, say, for the vortex shedding is $\tau_s \sim L/U_0$ [13]. As pointed out earlier, the thickness δ of a steady diffusion layer is $\delta = (DL^2/U_0)^{1/3}$. The time scale, τ_a, say, for the diffusion layer to adjust to changes in external conditions can thus be estimated as $\tau_a \sim \delta^2/D$. These estimates give

$$\frac{\tau_s}{\tau_a} \sim Pe^{-1/3} \ll 1 \tag{19}$$

Thus, the slow adjustment of the diffusion layer cannot keep up with the rapid changes in the velocity field caused by vortex shedding. As a consequence, the instantaneous mass transfer will deviate very little from its temporal mean value. This state of affairs is clearly illustrated in Fig. 4. In the rear part of the surface of the cylinder, Fig. 4(a), on the one hand, shows that the instantaneous velocity gradient is highly asymmetric with respect to the horizontal. Figure 4(b), on the other hand, shows that the instantaneous isoconcentration lines are almost perfectly symmetrical apart from some weak differences outside the upper and lower points of separation.‡

Periodically, two eddies are formed downstream the cylinder whose sizes are alternatively growing and decreasing. There is a region, about 150° from the front side, where the velocity is low, resulting in a locally lower mass flux.

As the separation point for $Re = 200$ is located at $\theta \approx 110°$ and that for $Re = 10$ is at $\theta \approx 150°$, the relative contribution to the net mass transport from the complicated near wake region is larger in the former case (cf. Fig. 2 with Fig. 6). It can be noted that for $Re = 200$, the near wake flow is sufficiently strong to enforce boundary layer behaviour of the concentration field on the rear part of the cylinder, which was found not to be the case at $Re = 10$ (cf. Fig. 4(b) with Fig. 3.).

The flux distribution has been used to compute the variation of the thickness of the deposit layer as shown schematically in Fig. 7. It should be noted that the possible modifications of the flow, due to the changes in the shape of the cylinder caused by inhomogeneous coating, has been neglected because of the very small thickness of the layer, typically a few micrometers, in comparison with the radius of the cylinder. The poor deposition in the neighbourhood of the mean location of the points of separation is noteworthy.

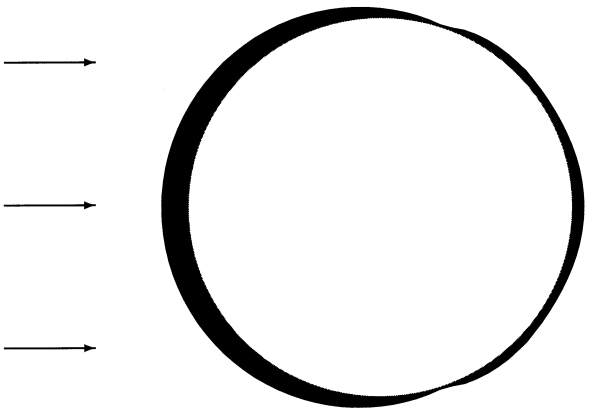

Fig. 7. Amplified deposit layer thickness. Limiting- current state at $Re = 200$.

‡The variation of the location of the separation point is small, about $\pm 10°$ [27]. Figure 4(b), where these points are located almost symmetrically, is thus not atypical.

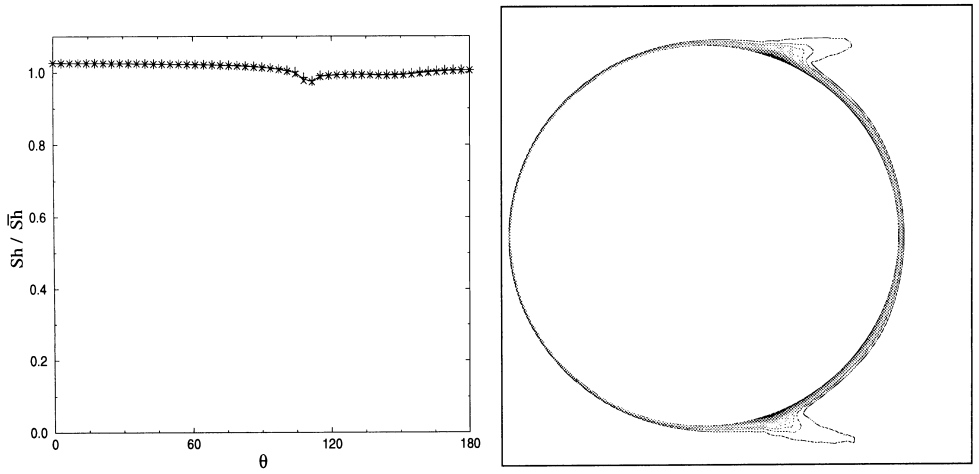

Fig. 8. (a) Nondimensional flux distribution. σ is the standard deviation. (–) mean, (+) mean + $\sigma/2$, (×) mean − $\sigma/2$. (b) Concentration field. $\kappa = 0.03$. $Re = 200$.

An obvious strategy in electrochemical process engineering is to operate under mass transport controlled, limiting-current, conditions, as the production rate should be maximized. However, there are cases when operation at the limiting current may not be desirable [21], for example, for reasons of energy consumption, homogeneity and quality of the deposit. Therefore, a case controlled by the charge transfer resistance at the surface of the cylinder was investigated. Results from simulations for $Re = 200$ and $\kappa = 0.03$ are shown in Fig. 8. For practical purposes, the mass transfer is homogeneous. The price paid for this homogeneity is low mass transfer. The ratio between the net mass transfer for $\kappa = 0.03$ and that at the limiting-current is only 2.7%.

For industrial applications in electroplating, the unsteadiness of the flow is of less interest. The important quantity is the thickness of the deposit layer, which is a time integrated quantity. To compute the thickness of the layer, the flow field must be simulated for a sufficiently long time and the flux must be integrated in time, as was done to obtain the necessary data for Fig. 7. Such computations are usually time consuming. To reduce the calculation time, a numerically enforced steady solution can be computed. In some applications, such artificial solutions may serve as reasonable approximations. However, this is not so in the present case. To enforce a steadiness in the computations, a first-order accurate hybrid differencing scheme was used for the discretization of the convective terms. An artificially steady solution can be obtained at considerably lower cost than an unsteady solution. The velocity field for such a steady solution is shown in the Appendix.

The mass flux obtained by an enforced steadiness of the velocity field is indicated by circles in Fig. 9. This graph also shows the mass flux distribution obtained by averaging the time-dependent solution. The position of the separation point is predicted correctly. On the other hand, the steady velocity field gives an accurate flux distribution only upstream of the separation point, not downstream. The steady state calculation predicts two large eddies behind the cylinder, with a flow towards the cylinder in the

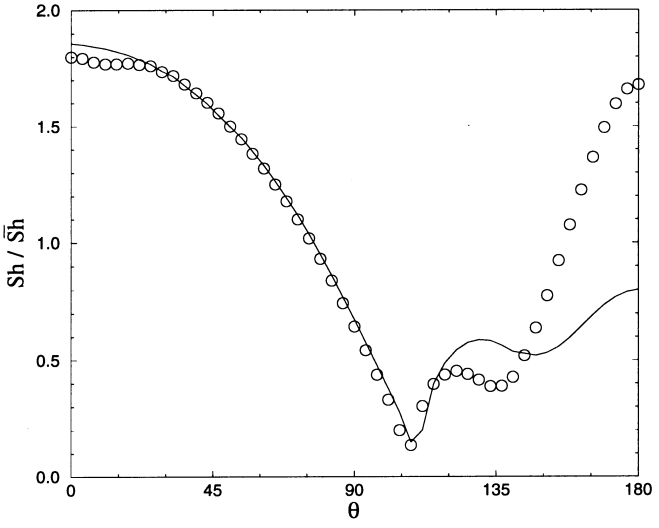

Fig. 9. Flux distribution for the limiting-current state at $Re = 200$. (—) Unsteady and (○) steady solutions.

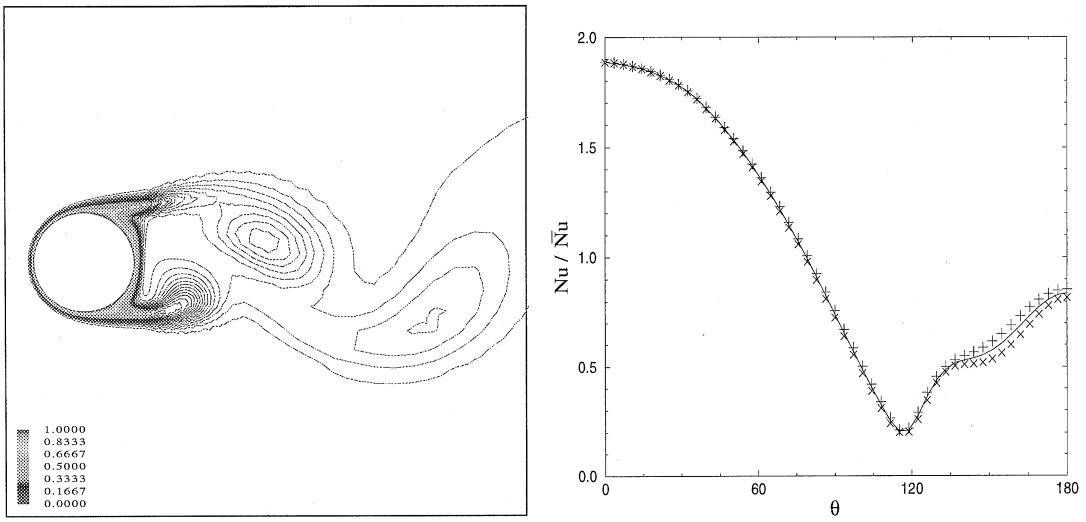

Fig. 10. (a) Temperature field. (b) Heat flux distribution for water. UWT at $Re = 200$. σ is the standard deviation. (–) mean, (+) mean $+ \sigma/2$, (×) mean $- \sigma/2$.

middle. This directed flow decreases the boundary layer thickness and thereby increases the mass flux to the cylinder surface. More complex dynamics are predicted by the time dependent calculations where the flow is less directed.

It is of interest to compare the influence of oscillations on mass transfer with their influence on heat transfer at the same Reynolds number $Re = 200$. Calculations were done for the case of water flow around the cylinder in a uniform wall temperature case at Prandtl number of 7, with a temperature difference of 10 °C between the cylinder wall and the inlet flow. The resulting isothermal lines and the heat flux distribution are shown in Fig. 10(a) and (b). Heat flux is given, with dimensionless variables, in terms of the Nusselt number Nu ($Nu = \partial T/\partial r$ at the wall), normalized by its mean value over the cylinder averaged in time, $\overline{Nu}$. In the case of heat flux, the oscillations are about 10% of the mean heat flux, that is to say ten times more than for the mass transfer case. This obvious difference can be attributed to large differences between the Schmidt number in the case of mass transfer and the Prandtl number for the case of heat transfer.

5. Conclusion

Cathodic limiting-current conditions are widespread in electroplating, specially under forced convection. The present numerical simulations verify that the mass transport limitation is maximum under such conditions and in contrast, for low reaction rates, it is not limiting.

The transition from low Reynolds steady flow to periodic unsteady conditions is not passed to the concentration field and its resulting mass flux distribution. This field keeps an almost steady symmetric pattern with two zones of maximum cation depletion situated near the separation point positions. This characterizes high Schmidt number conditions and is particularly remarkable if compared with corresponding influence of flow oscillations on a heat transfer case.

The consequence of increasing the stream velocity, and thus the convective 'strength', is an obvious increase of the global mass flux rate (i.e. the deposition rate) but, as the wake region gets larger in the downstream part of the cylinder, the low deposited area becomes larger too.

The enforced steady solution that can be obtained numerically for a Reynolds number of 200 gives a good idea of the extent of the nonhomogeneous near wake region but with non-negligible deviation from the actual unsteady result for the flux distribution in that region.

The results can be visualized by concentration fields or flux distribution. The latter can be used for illustration of the deposit layer thickness. A good homogeneity of the deposit is desirable for obvious reasons of quality but also for nonnegligible savings on deposited metal. The numerical prediction can then be used, for instance, to decide on first guess conditions for a series of tests when starting the plating of a new workpiece or, more generally, to help in understanding and diminishing the non-homogeneity in the deposit.

This new step in numerical methods applied to electroplating process is encouraging despite its limitation to a 2D case at intermediate Reynolds numbers. A natural extension is the study of 3D effects due to geometry configuration or higher flow rates.

6. Appendix

6.1. *Validations*

The case of heat transfer around a cylinder, which was studied in Section 4, can be used for validation of the code. Here, a detailed comparison is made with

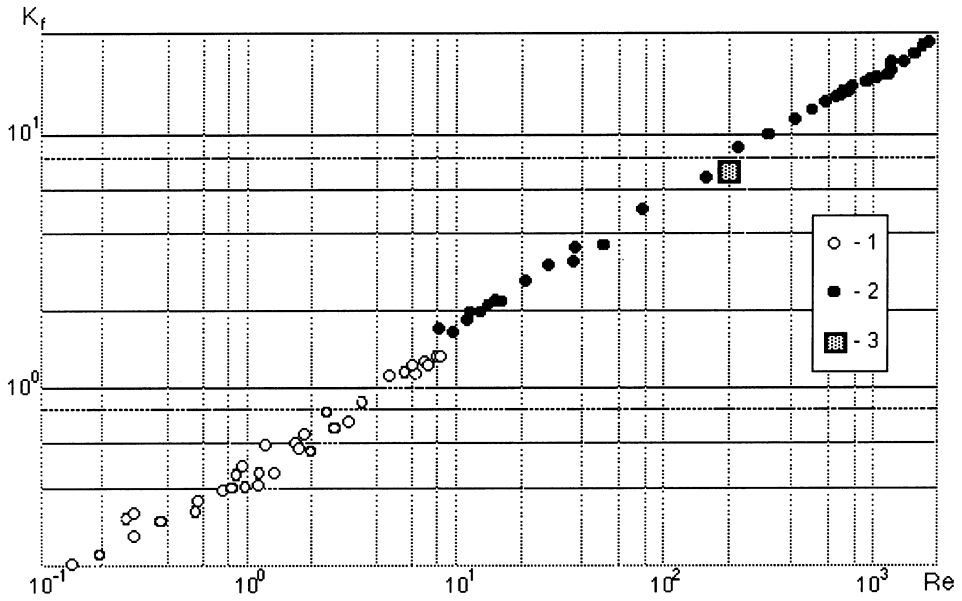

Fig. 11. Heat transfer of cylinders in low range of Re : (1) Davis [28]; (2) Žukauskas [29]; (3) present work.

available experimental data in the literature. The Reynolds number is 200, and the wall temperature is uniform, 10 °C over the fluid temperature. The resulting average heat transfer coefficient is presented in Fig. 11 where comparison is made with data from Žukauskas [14].

The nondimensional frequency of oscillations, denoted f, is usually presented by way of the Strouhal number defined by

$$St = \frac{2fR}{U} \tag{20}$$

The Strouhal number can be estimated as 0.195, where the frequency is found from the recorded oscillations in the drag force as shown in Fig. 12. The numerical work of Ha Minh *et al.* [30] reports a value of Strouhal number $St = 0.19$. Braza *et al.* [27] found 0.20. Experimental results from Roshko in 1954 [31] give values in the range of 0.18–0.20, for the same Reynolds number.

An experimental value for the drag coefficient C_D, which is found by integration of the forces acting on the cylinder, is 1.4, [e.g. 32]. This value must be compared to 1.47 in the present simulation.

6.2. *Steady solution for* $Re = 200$

The velocity field of the steady symmetric solution at $Re = 200$ is shown in Fig. 13. A hybrid central/upwind scheme was used in order to obtain a con-

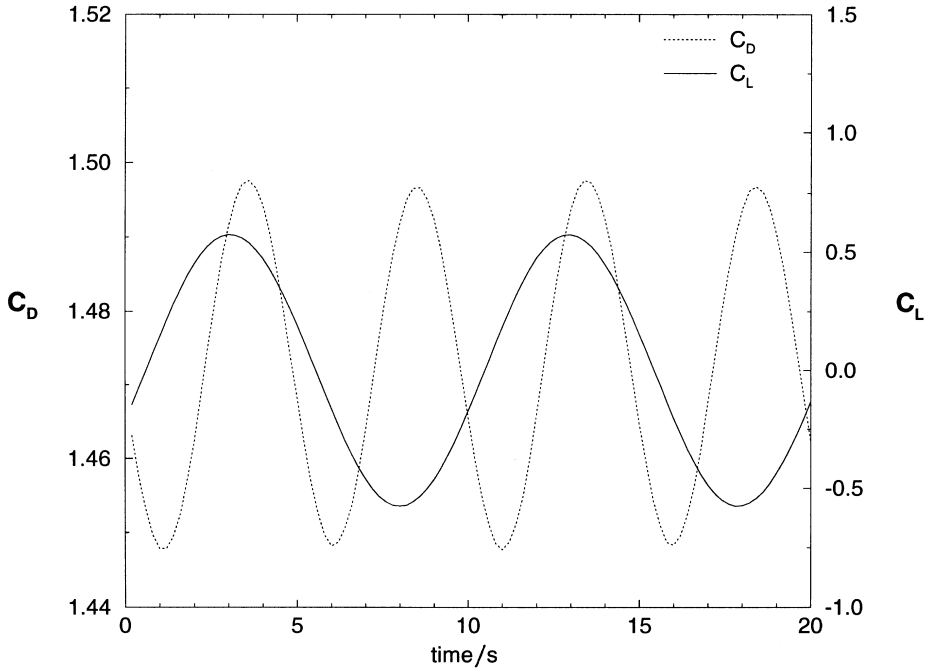

Fig. 12. Time dependent lift and drag coefficients after establishment time at $Re = 200$.

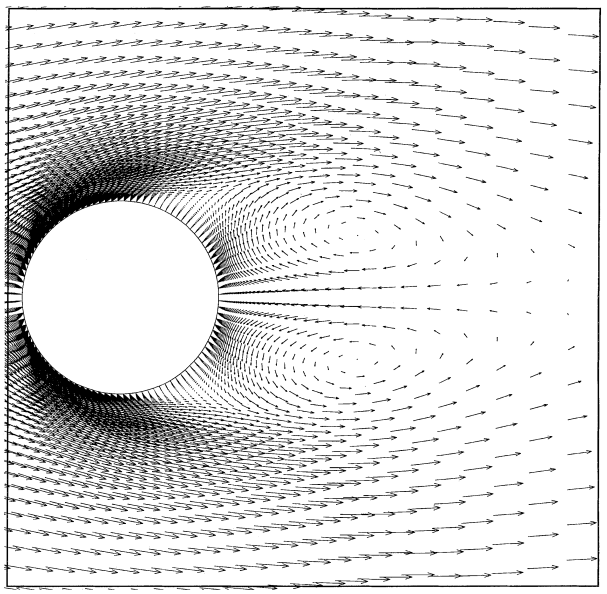

Fig. 13. Velocity field at $Re = 200$. Steady calculation.

vergence of the iterations, giving this artificial steady solution.

References

[1] V. S. Bagotzky, 'Fundamentals of Electrochemistry', Plenum Press, New York (1993), p. 404.
[2] 'Metal Finishing Guidebook and Directory', Elsevier Science Publications, New York, USA, published annually.
[3] F. C. Walsh, *Trans. Inst. Metal Finish.* **70**(1) (1992) 50.
[4] E. Raub and K. Müller, 'Fundamentals of Metal Deposition', Elsevier Publishing, Amsterdam (1967) ch. 5.
[5] A. F. Averill and H. S. Mahmood, *Trans. Inst. Metal Finish.* **74**(1) (1996) 11.
[6] V. G. Levich, 'Physicochemical Hydrodynamics', Prentice-Hall, Englewood Cliffs, NJ (1962) ch. 2, ch. 6.
[7] J. S. Newmann, 'Electrochemical Systems', Prentice-Hall, Englewood Cliffs, NJ (1974) ch. C, ch. D.
[8] M. J. Lighthill, *Proc. R. Society Lond.* **A202** (1950) 359.
[9] A. Acrivos, *Physics of Fluids* **3** (1960) 657.
[10] T. J. Hanratty and J. A. Campbell, 'Fluid Mechanics Measurements' (edited by R. J. Goldstein), Hemisphere, Washington (1983), p. 559.
[11] P. Olivas, 'Écoulements autour de trois cylindres en ligne: Mesure du gradient pariétal sur le cylindre central', Mémoire de D.E.A. de l'I.N.P. Grenoble (1994).
[12] G. K. Batchelor, 'An Introduction to Fluid Dynamics', Cambridge University Press (1967), ch. 4.
[13] D. J. Tritton, 'Physical Fluid Dynamics', Oxford Science Publications, New York (1988), ch. 3.
[14] A. Žukauskas and J. Žiugžda, 'Heat Transfer of a Cylinder in Crossflow', edited by G. F. Hewitt, Hemisphere Publ. Washington (1985) 136.
[15] P. Legentilhomme and J. Legrand, *J. Appl. Electrochemistry* **20** (1990) 216.
[16] R. E. Sioda, *B. Electrochem.* **4** (1988) 383.
[17] H. G. Dimopoulos and T. J. Hanratty, *J. Fluid Mechanics* **33** (1968) 303.
[18] J. Josserand, 'Modélisation des processus de "l'électrodéposition continue"', Thèse Docteur de l'I.N.P. Grenoble (1994), p. 84.
[19] E. Gileadi, 'Electrode Kinetics', VCH, New York (1993) pp. 3, 57, 351.
[20] F. C. Walsh, *Trans. Inst. Metal Finish.* **70** (1992) 95.
[21] D. Pletcher and F. C. Walsh, 'Industrial Electrochemistry', Chapman & Hall, London (1990) ch. 1.2, ch. 2.5, ch. 2.6.
[22] S. C. R. Dennis and G. Z. Chang, *J. Fluid Mechanics* **42** (1970) 471.
[23] J. S. Son and T. J. Hanratty, *ibid.* **35** (1969) 353.
[24] J. P. Celis, M. De Bonte and J. R. Roos, *Trans. Inst. Metal Finish.* **72**(2) (1994) 89.
[25] Computational Fluid Dynamics Services, Harwell Laboratory: *CFX-F3D User Manual*, Oxfordshire, UK (1995).
[26] V. Sobolík and O. Wein, *Int. J. Heat Mass Transfer* **34** (1991) 1929.
[27] M. Braza, P. Chassaing and H. Ha Minh, *J. Fluid Mechanics* **165** (1986) 79–130.
[28] A. H. Davis, *Phil. Mag.* **47** (1924) 282.
[29] A. Žukauskas, *Advances in Heat Transfer* **8** (1972) 93.
[30] H. Ha Minh, H. Boisson and G. Martinez, *J. Heat Transfer* **13** (1980) 35.
[31] A. Roshko, NACA report 1191 (1954).
[32] H. Schlichting, 'Boundary Layer Theory', McGraw-Hill, New York (1979), p. 17.